ISSN 1560-3547, Regular and Chaotic Dynamics, 2016, Vol. 21, No. 2, pp. 160–174. © Pleiades Publishing, Ltd., 2016.

Verification of Hyperbolicity for Attractors of Some Mechanical Systems with Chaotic Dynamics

Sergey P. Kuznetsov[1,2,3*] and Vyacheslav P. Kruglov[2,4]**

[1] *Udmurt State University, ul. Universitetskaya 1, Izhevsk, 426034, Russia*

[2] *Kotelnikov's Institute of Radio-Engineering and Electronics of RAS, Saratov Branch, ul. Zelenaya 38, Saratov, 410019 Russia*

[3] *Saratov State University, ul. Astrakhanskaya 83, Saratov, 410012 Russia*

[4] *Saratov State University, ul. Astrakhanskaya 83, Saratov, 410012, Russia*

Received December 06, 2015; accepted February 15, 2016

Abstract—Computer verification of hyperbolicity is provided based on statistical analysis of the angles of intersection of stable and unstable manifolds for mechanical systems with hyperbolic attractors of Smale – Williams type: (i) a particle sliding on a plane under periodic kicks, (ii) interacting particles moving on two alternately rotating disks, and (iii) a string with parametric excitation of standing-wave patterns by a modulated pump. The examples are of interest as contributing to filling the hyperbolic theory of dynamical systems with physical content.

MSC2010 numbers: 37D20, 37D45, 70G60, 70Q05

DOI: 10.1134/S1560354716020027

Keywords: dynamical system, chaos, attractor, hyperbolic dynamics, Lyapunov exponent, Smale – Williams solenoid, parametric oscillations

1. INTRODUCTION

Hyperbolic theory is a part of the modern theory of dynamical systems delivering a rigorous mathematical justification of chaotic behavior in deterministic systems, both in the discrete time case (iterative maps — diffeomorphisms) and in continuous time (flows) [1–6].

The objects of study are uniformly hyperbolic invariant sets composed exclusively of saddle trajectories in the phase space of dynamical systems. For all points on such a trajectory, in the space of infinitesimal perturbations (tangent space), one can define a subspace of vectors exponentially decreasing in norm in the course of the evolution forward in time, and a subspace of vectors exponentially decreasing during evolution in reverse time. In flow systems, additionally, a neutral subspace is introduced to take into account perturbations directed along the trajectory, which do not grow or decrease on average. An arbitrary vector of an infinitesimal perturbation is required to allow representation as a linear combination of vectors related to these subspaces. The set in the phase space composed of orbits which approach the reference trajectory in forward time is called the *stable manifold*. Similarly, the unstable manifold is defined as a set approaching the reference trajectory in reverse time. Tangencies of the stable and unstable manifolds for the hyperbolic invariant sets are excluded; only intersections at nonzero angles are allowed.

For dissipative systems the hyperbolic theory introduces a special type of attracting invariant sets, the uniformly hyperbolic chaotic attractors. An example is the Smale – Williams attractor. Consider a region in the form of a torus in the three-dimensional state space and assume one step of the transformation is that we stretch it twice with simultaneous transversal compression, fold it to

* E-mail: spkuz@yandex.ru

** E-mail: kruglovyacheslav@gmail.com

produce a double loop, and put it inside the original torus. This procedure is repeated many times. At each step the volume of the object decreases (this means that the mapping is dissipative), and the number of turns is doubled, and in the limit tends to infinity. The result is the formation of the so-called solenoid, which possesses a Cantor-like structure in the transversal direction. An obvious generalization is folding a loop with another number of coils (three or more) in one step of the construction. Chaotic dynamics on such attractors are determined by the evolution of the angular coordinate according to expanding the circle map, or the Bernoulli map $\theta_{n+1} = M\theta_n \,(\mathrm{mod}\, 2\pi)$ with integer factor $M \geqslant 2$.

A fundamental mathematical fact is that the uniformly hyperbolic attractors are rough, or structurally stable [1–6]. After Andronov and Pontryagin had introduced the notion of roughness (suitable for systems with regular dynamics) [7, 8], it was commonly accepted to postulate that just the rough systems are of real interest and importance as they manifest low sensitivity to setting parameters and functional characteristics of elements, to manufacturing imperfections, noise, errors, etc. [9–13].

The trouble is that, considering numerous realistic examples of chaotic systems of different nature (mechanics, fluid dynamics, electronics, chemical kinetics [14–21]), we do not meet uniformly hyperbolic attractors there. In textbooks and reviews on dynamical systems such attractors are presented exclusively by artificially constructed mathematical examples, such as DA-attractor of Smale, Plykin attractor, and the aforementioned Smale – Williams solenoid [1–6].

The situation that the question of occurrence of the hyperbolic chaos in nature and its practical applications in technology has been overlooked seems strange and unacceptable in view of the declared priority of rough systems. Indeed, for any application of chaos, the class of systems with uniformly hyperbolic attractors looks preferable in this sense. One more potentially interesting and important property is the possibility of complete symbolic description of trajectories belonging to the uniformly hyperbolic attractors with a finite alphabet based on the Markov partitions [3, 4]. It establishes a fundamental relationship of the hyperbolic dynamics with information and coding theory [22], and may be of importance for possible information and communication applications.

In the absence of ready-to-use examples in nature and technology, it seems productive to turn to purposeful constructing systems with hyperbolic dynamics by means of the toolbox of physics and theory of oscillations and waves (oscillators, particles, fields, interactions, feedback circuits, etc.). In this regard, certain progress has been achieved recently, and many realizable physically motivated systems with hyperbolic attractors have been offered [23–36]. Among them, mechanical examples may be of particular interest as they are easily perceived and interpreted due to our everyday experience.

Naturally, physical and technical devices are not specially suited to admit direct mathematical proofs. Nevertheless, confident confirmation of hyperbolicity may be of practical significance to exploit properly the relevant results of the mathematical theory, like description in terms of Markov partitions or structural stability of the chaotic attractors. So, it is vital to employ numerical instruments for computational tests of the hyperbolicity.

The present paper is devoted to the development and application of such a tool based on the verification of transversality of stable and unstable manifolds for trajectories on attractors, which is a key basic property of the hyperbolicity. In Section 2 we consider simple examples (torus map and Hénon map) to clarify the sense of transversal disposition of the stable and unstable manifolds required for the hyperbolicity by their visualization accessible in the two-dimensional case. In Section 3 we explain a more formal alternative approach based on statistical analysis of distributions of angles of intersections of the unstable and stable subspaces of perturbation vectors for the phase trajectories. Its advantage is the possibility of generalization for higher dimensions of the state space. In Section 4, which is the main part of the article, this approach is applied to some mechanical systems suggested earlier as possible candidates for the occurrence of hyperbolic attractors [35, 51].

2. VISUAL VERIFICATION OF TRANSVERSALITY OF STABLE AND UNSTABLE MANIFOLDS FOR 2D MAPS

The consideration we start is based on simple and general reasoning concerning dynamics near invariant sets in the phase space of dynamical systems.

Let the system we analyze have a chaotic attractor A. Selecting a point $\tilde{\mathbf{x}} \in A$ relating to some distant time in the past $t_0 - T$ (relative to the instant of observation t_0), consider an ensemble of initial conditions in its small ε neighborhood. Then the images of the initial points at t_0 will arrive practically at the attractor; it is so because of definition of A as a set attracting all neighbor orbits. (The accuracy of the approach to A is determined by ε, time T, and negative Lyapunov exponents of the attractor.) On the other hand, these image points (with a certain accuracy) relate to the unstable manifold. Indeed, considering the dynamics on the orbits in backward time, we see them approaching the attractor and gathering in the ε neighborhood of $\tilde{\mathbf{x}}$.

Alternatively, we can select a point $\bar{\mathbf{x}} \in A$ at distant future $t_0 + T$ and consider the evolution of the ensemble of states in its neighborhood backward in time, which gradually depart from A. (Instead of attraction in forward time we have repelling in backward time provided by the negative Lyapunov exponents.) Then, at t_0 the states will be placed along the stable manifold, which is by definition a set of trajectories approaching A in direct time.

A simple graphical presentation of the stable and unstable manifolds is accessible if we deal with a two-dimensional map $\mathbf{x}_{n+1} = \mathbf{f}(\mathbf{x}_n)$, which is supposed to allow backward iterations as well. The unstable manifolds are one-dimensional and coincide with the filaments forming the structure of the attractor; so, to judge about transversality, it is sufficient together with the attractor to draw only the *stable manifolds*, which are one-dimensional too. The pictures obtained in this way are illuminating and convincing to conclude qualitatively about the absence or presence of the tangencies, and respectively, about the occurrence or violation of the hyperbolicity.

To depict the stable manifolds with computer, we proceed as follows. First, for an arbitrary chosen point on the attractor $\mathbf{x}$ we generate the image by K-fold application of the map, $\bar{\mathbf{x}} = \mathbf{f}^K(\mathbf{x})$. Then, with random initial conditions defined by vectors $\bar{\mathbf{y}}$ in a small ε neighborhood of $\bar{\mathbf{x}}$, by backward iterations of the map we get a set of points $\mathbf{y} = \mathbf{f}^{-K}(\bar{\mathbf{y}})$, which represent graphically, with a certain accuracy, the stable manifold containing the initial state $\mathbf{x}$. Formally speaking, the precision with which the manifolds are depicted grows fast with increase of K and respective decrease of ε, but an actual selection of these quantities implicates a compromise between the graphical accuracy and the numerical errors accumulating as ε is too small and K is too large. For concrete maps, it is not difficult to select the parameters of the algorithm to reach the graphical presentation accuracy comparable with a pixel size of the computer plot, which is certainly sufficient for the qualitative analysis.[1)]

Our first example will be the map [28, 36]:

$$\begin{aligned} p_{n+1} &= p_n + q_n + k\Big(\sin p_n + \frac{1}{2}\sin 2p_n\Big) \pmod{2\pi}, \\ q_{n+1} &= p_n + 2q_n + k\Big(\sin p_n + \frac{1}{2}\sin 2p_n + \sin q_n + \frac{1}{2}\sin 2q_n\Big) \pmod{2\pi}. \end{aligned} \tag{2.1}$$

At $k = 0$ it is the hyperbolic automorphism of torus, known as the Arnold cat map. At appropriately chosen nonzero k it manifests a hyperbolic attractor called DA-attractor of Smale (DA stands for "Derived-from-Anosov"). In Fig. 1a the attractor at $k = 0.7$ is shown in red, and the family of curves representing the stable manifolds is shown in black. One can see clearly that the black curves intersect the filaments of the attractor transversally (nonzero angles). Note that the family of the stable manifolds visually looks representative: one can easily imagine intermediate missed curves, and the transversality obviously takes place everywhere.

For comparison, in Fig. 1b a picture is drawn in the same manner for the chaotic attractor of the Hénon map [37]

$$x_{n+1} = 1 - ax_n^2 + by_n, \;\; y_{n+1} = x_n \tag{2.2}$$

[1)]Say, for the examples (2.1) and (2.2) discussed here, it was taken $\varepsilon \sim 10^{-5}$ and $K \sim 10$.

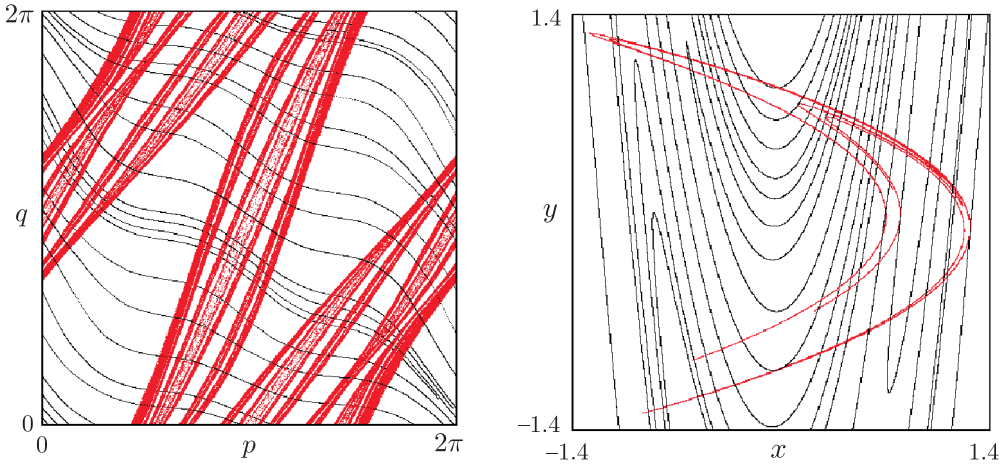

Fig. 1. Uniformly hyperbolic attractor of the map (2.1) at $k = 0.7$ (a) and nonhyperbolic attractor of Hénon map (2.2) at $a = 1.4$, $b = 0.3$ (b) shown in red. Families of stable manifolds computed as explained in the text at representative points of the attractors are shown in black.

at a=1.4, b=0.3. Again, the families of the stable manifolds are obviously representative; one can easily supplement them mentally with intermediate curves. However, the picture looks essentially different. Namely, the stable manifolds are disposed in such a way that the tangencies with filaments of the attractors occur inevitably.

3. ANALYSIS OF DISTRIBUTION OF INTERSECTION ANGLES OF STABLE AND UNSTABLE SUBSPACES OF PERTURBATIONS. MAIN IDEA AND SIMPLE EXAMPLES

For maps of higher dimensions it is problematic to give a graphically convincing evidence for mutual placement of the manifolds. An alternative approach adaptable for these cases may be based on consideration of statistical distribution of angles of intersection of stable and unstable subspaces in tangent vector space (perturbation vector space) tracing these angles along a representative phase trajectory on the analyzed invariant set. Such a method was originally suggested and developed for saddle chaotic orbits in [38]. Afterwards, it was applied for chaotic attractors as well [39–42], including attractors of Smale – Williams and Plykin type of physically realizable systems [23, 24, 29].

The criterion is convenient to use in an elegant formulation of [41]; here we restrict ourselves to the case when the unstable manifolds are one-dimensional (one positive Lyapunov exponent), which is sufficient for our purposes.[2)]

First, consider the discrete time case.

The first stage is to obtain a sufficiently long time series $\mathbf{x}_n$ of vectors belonging to the phase space of dimension N of the analyzed map $\mathbf{x}_{n+1} = \mathbf{f}(\mathbf{x}_n)$ by iterations of this map. It will be regarded as a reference orbit on the attractor.

Next, we take a linearized equation for the perturbation vector $\tilde{\mathbf{x}}_{n+1} = \mathbf{f}'(\mathbf{x}_n)\tilde{\mathbf{x}}_n$, where $\mathbf{f}'(\mathbf{x}_n)$ is the Jacobi matrix of size $N \times N$ composed of partial derivatives, and perform iterations along the reference trajectory $\mathbf{x}_n$ with normalization of the vector $\tilde{\mathbf{x}}_n$ at each step n to exclude divergences. The result is a set of unit vectors $\{\tilde{\mathbf{x}}_n^0\}$. Then we have to pass the same reference trajectory in reverse time and determine a stable vector subspace at each n as a subspace of vectors expanding in the reverse time. In earlier versions of the algorithm it was provided by tracing a collection of an appropriate number of perturbation vectors in reverse time with taking measures to exclude domination of one or more directions of fast growth (Gram-Schmidt orthogonalization). Instead of

[2)] The method of statistical analysis for the angles may be generalized for invariant sets with stable and unstable manifolds of any dimension considering the so-called principal angles of intersection for the respective multidimensional stable and unstable subspaces of infinitesimal perturbation vectors [41], but this generalization goes beyond the scope of the present article.

this, and it was the novation introduced in [41], one can deal with a single vector $\tilde{\mathbf{u}}$ corresponding to the orthogonal complement to the stable subspace. To do so, we have to perform iterations along the reference trajectory in reverse time for a linear equation $\tilde{\mathbf{u}}_n = [\mathbf{f}'(\mathbf{x}_n)]^T \tilde{\mathbf{u}}_{n+1}$, which contains the transposed Jacobi matrix. With normalization at each step, we obtain a set of unit vectors $\{\tilde{\mathbf{u}}_n^0\}$.

In the case of continuous time (flow) we start by calculating the reference orbit $\mathbf{x}(t)$ on the attractor, tracing a solution of the differential equation $\dot{\mathbf{x}} = \mathbf{F}(\mathbf{x}, t)$ over a sufficiently long time interval. Then take the linearized equation for the perturbation vector $\dot{\tilde{\mathbf{x}}} = \mathbf{F}'(\mathbf{x}(t), t)\tilde{\mathbf{x}}$ and solve it numerically along the reference trajectory forward in time with normalization of the vector $\tilde{\mathbf{x}}$ at each step of the integration scheme and obtain a set of unit vectors $\{\tilde{\mathbf{x}}_n^0\}$. Next, the integration is performed in reverse time along the same reference orbit using the conjugate linear equation $\dot{\tilde{\mathbf{u}}} = -[\mathbf{F}'(\mathbf{x}(t), t)]^T \tilde{\mathbf{u}}$. With normalization, it provides a set of vectors $\{\tilde{\mathbf{u}}_n^0\}$, each defines the orthogonal complement to the stable subspace of the perturbation vectors at a reference point. These vectors also are normalized to unity in the course of the computations.

The last stage, common in the discrete and continuous time cases, is evaluation of the angles ϕ between the one-dimensional unstable subspace and the stable subspace at each recorded step of the trajectory. Namely, we calculate the angle $\beta_n \in [0, \pi/2]$ between the vectors $\{\tilde{\mathbf{x}}_n^0\}$ and $\{\tilde{\mathbf{u}}_n^0\}$: $\cos\beta_n = \left|\tilde{\mathbf{u}}_n^0(t) \cdot \tilde{\mathbf{x}}_n^0(t)\right|$, and set $\phi_n = \pi/2 - \beta_n$. The final result is a histogram for the statistical distribution of the angles.

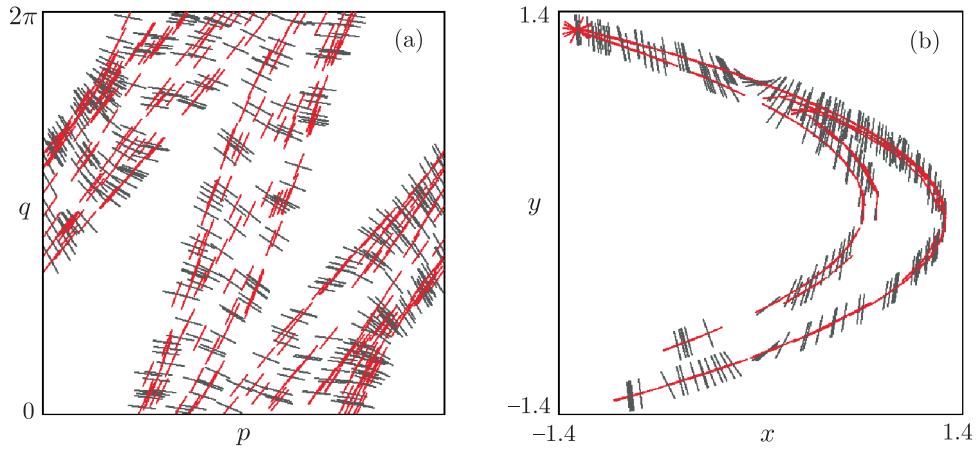

Fig. 2. Two-dimensional state space diagrams, where directions of vectors of stable and unstable subspaces at representative points of attractors are indicated in black and red, respectively, for the map of torus (2.1) at $\varepsilon = 0.7$ (a) and the Hénon map (2.2).

For illustration, Fig. 1 shows diagrams on the planes of dynamical variables for the torus map and Hénon map. On these plots the directions of vectors belonging to stable and unstable subspaces are indicated at representative points of the attractors. Red color corresponds to directions of the vectors $\tilde{\mathbf{x}}$ and black shows directions orthogonal to the vectors $\tilde{\mathbf{u}}$ as computed by the above algorithm. A comparison of these diagrams with Fig. 1 clarifies a relationship of the visual estimate of the presence of transversality or tangencies for the manifolds in the previous section with the approach we consider now. As is seen, mutual locations of the red and black segments precisely correspond to the tangent directions to the stable and unstable manifolds, respectively, and therefore the same is true for the angles of the intersections. Statistical analysis of these angles is just the content of the approach to verification of the hyperbolicity we will use in the rest of the article.

Figure 3 shows histograms of the statistical distributions of the intersection angles for the attractors of the torus map and the Hénon map.

For the hyperbolic attractor of the torus map (2.1) a clearly visible gap exists separating the distribution from zero angles (panel (a)). It is illuminating to compare this picture with that relating to an attractor which is not uniformly hyperbolic. The histogram for the Hénon attractor (panel (b)) indicates statistically significant nonvanishing probability density around zero angles.

It implies the occurrence of tangencies of the stable and unstable manifolds in agreement with the visual estimate from Fig. 1b.[3)]

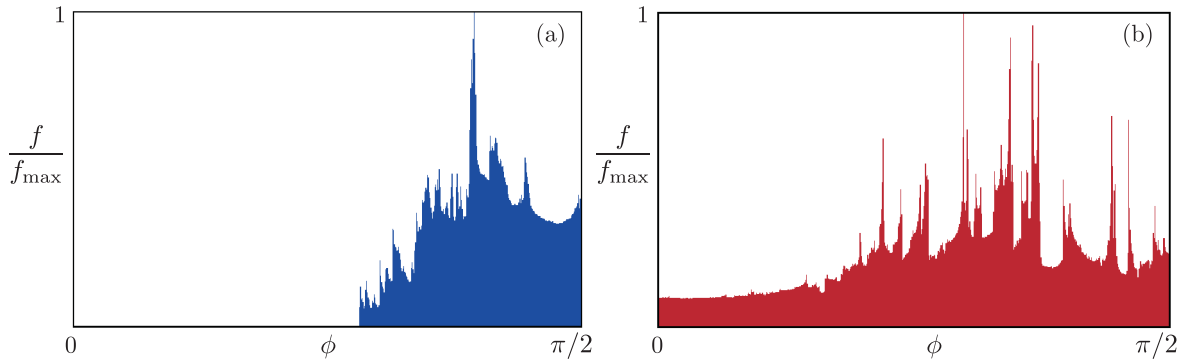

Fig. 3. Histograms for distributions of intersection angles for stable and unstable subspaces for the uniformly hyperbolic DA-attractor of the map (2.1) at $\varepsilon = 0.7$ (a) and for the nonhyperbolic attractor of the Hénon map (2.2) at $a = 1.4$, $b = 0.3$ (b).

4. VERIFICATION OF HYPERBOLICITY OF SOME MECHANICAL SYSTEMS

4.1. Particle Motion on a Plane under Periodic Kicks

Situations of particle motion on a plane under periodic kicks associated with attractors of Smale–Williams type in the stroboscopic map were proposed and studied numerically in [43]. Here we consider a slightly different version introduced in the later work [35], which is apparently better suited for possible experimental realizations.

Consider a particle of unit mass on the plane $(x,\ y)$ in a stationary potential field $U(x,y) = -\frac{1}{2}\mu(x^2+y^2) + \frac{1}{4}\mu(x^2+y^2)^2$ possessing rotational symmetry about the origin, with minimum on the unit circle. We assume that an additional force field with potential $V(x,y) = \frac{1}{2}(x^2+y^2) - \frac{1}{3}x^3 + xy^2$ is switched on and off periodically with time interval T, producing short-time kicks of magnitude and direction depending on the instantaneous position of the particle. Also, we add the friction force proportional to the velocity; the friction coefficient is assumed to be unity for simplicity.

Given the initial state just before the n-th kick $\mathbf{x}_n = \{x,\ \dot{x},\ y, \dot{y}\}_{t=nT-0}$, one can determine the state before the next, n+1-th kick from the solution of the equations

$$\ddot{x} + \dot{x} = \mu x(1-x^2-y^2), \quad \ddot{y} + \dot{y} = \mu y(1-x^2-y^2) \tag{4.1}$$

on a period T with the initial conditions determined by the state immediately after the kick:

$$\begin{aligned} x|_{t=nT+0} &= x_n,\ \ \dot{x}|_{t=nT+0} = \dot{x}_n - x_n + x_n^2 - y_n^2, \\ y|_{t=nT+0} &= y_n,\ \ \dot{y}|_{t=nT+0} = \dot{y}_n - y_n - 2x_n y_n. \end{aligned} \tag{4.2}$$

[3)] One can ask — may it happen that the criterion is valid on one trajectory but fails on another one on the same attractor? How long must a reference trajectory be considered to be sure that the histogram actually indicates the occurrence or absence of hyperbolicity? It must be clearly understood that the procedure does not offer a mathematical proof (even in the sense of a computer assisted one), but provides only a practical tool to judge about hyperbolicity or nonhyperbolicity. We suppose that the reference trajectory may be regarded as a typical orbit on the attractor in the same sense as it is assumed in other practical numerical procedures, like evaluation of Lyapunov exponents, or dimensions, or spectra. Concerning the duration of the processed trajectory, it may be chosen empirically to contain about 10^4 or 10^5 of characteristic time intervals (say, steps of the Poincaré map), with a visual estimate of the quality of the histograms obtained. Although errors in distinguishing hyperbolicity and nonhyperbolicity cannot be excluded completely, the practice of the calculations certainly confirms the usefulness of this computational tool. Say, the comparison of the concrete results for the considered examples of the torus map and the Hénon map certainly looks convincing (Fig. 3).

To explain the system functioning, consider a ring of particles resting initially on the unit circle with coordinates $x = \cos\varphi$ and $y = \sin\varphi$, $0 \leqslant \varphi < 2\pi$. After a kick each particle will get the momentum components $P_x = -x + x^2 - y^2$ and $P_y = -y - 2xy$ depending on the initial angle φ. Without taking into account the field U, the particles would stop due to the friction at the coordinates easily evaluated as

$$x' = x + P_x = x^2 - y^2, \quad y' = y + P_y = -2xy. \tag{4.3}$$

If we substitute $x = \cos\varphi$ and $y = \sin\varphi$, we get $x' = \cos\varphi'$ and $y' = \sin\varphi'$, where $\varphi' = -2\varphi$. This means that the particles settle down again on the unit circle, but a single bypass of the original ring corresponds to a twofold bypass of the newly formed ring in the opposite direction. Thus, for the angular coordinate we have the expanding circle map, or the Bernoulli map.

In Eqs. (4.1) parameter μ may be selected small enough; then, during the characteristic time of motion caused by a single kick, a displacement of the particle due to the potential field $U(x, y)$ is rather negligible. On the other hand, the period of kicks T may be assumed large enough to have time for the particle to approach the potential minimum of $U(x, y)$. These conditions are not strong and may be valid at least in a rough approximation. (It is so because of structural stability of the hyperbolic attractor we intend to construct.)

Relations (4.1) and (4.2) give rise to the four-dimensional Poincaré map $\mathbf{x}_{n+1} = \mathbf{f}(\mathbf{x}_n)$; the action of this map can be easily reproduced by means of numerical integration of the differential equations (4.1) by a computer program.

Figure 4 illustrates some results of numerical simulations at $\mu = 0.3$ and $T = 4$. Panel (a) depicts a typical trajectory of the particle. Panel (b) shows the attractor in the stroboscopic section as projected on the plane (x, y). It is the Smale – Williams solenoid because of the outlined topological property of the ensemble of particles after the evolution between the kicks, namely, the emergence of the loop bypassing the origin twice. Panel (c) shows the iterative diagram for the angular variable φ_n determined immediately before each successive kick. One can see that the angular coordinate behaves in accordance with the expanding circle map: one bypass of the circle for the preimage implies two detours for the image in the opposite direction.

The chaotic nature of the dynamics is confirmed by numerical evaluation of the Lyapunov exponents [44–46] for the Poincaré map:

$$\Lambda_1 = \quad 0.687, \ \Lambda_2 = -1.386, \quad \Lambda_3 = -3.000, \quad \Lambda_4 = -3.733\,. \tag{4.4}$$

Note that the largest exponent is close to $\ln 2$ in accordance with twice expanding transformation of the angular variable on each period of kicks.

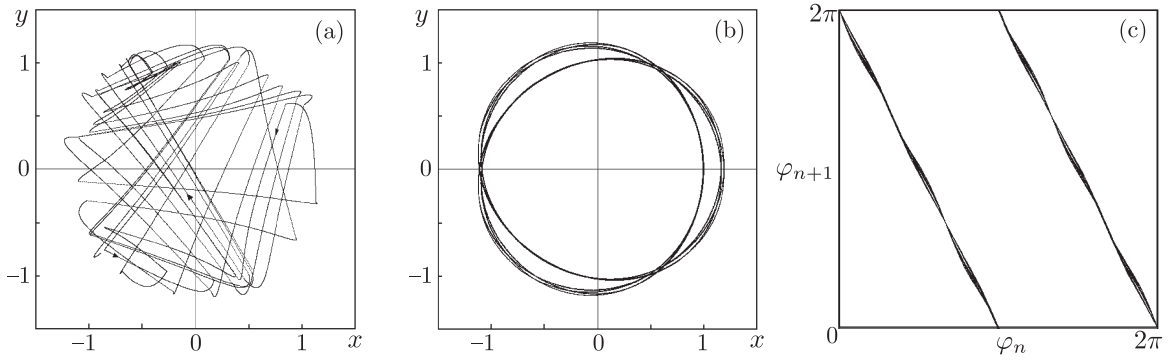

Fig. 4. A trajectory of the particle in the plane (x, y) produced by the model (4.1), (4.2) for 50 periods of the pulse driving (a), stroboscopic portrait of the attractor (b), and iteration diagram for the angular variable obtained from the numerical simulations at $\mu = 0.3$, $T = 4$.

Figure 5 shows results of testing the criterion of angles formulated in the previous section for the four-dimensional Poincaré map $\mathbf{x}_{n+1} = \mathbf{f}(\mathbf{x}_n)$ of the model (4.1), (4.2), via computation of the angles between unstable and stable subspaces on a long reference orbit on the attractor at $\mu = 0.3$, $T = 4$. Here the numerically obtained histogram is plotted, which clearly demonstrates the absence

of angles close to zero; this means that no tangencies of stable and unstable manifolds occur, and agrees with the conjecture that the attractor of the Poincaré map is hyperbolic.

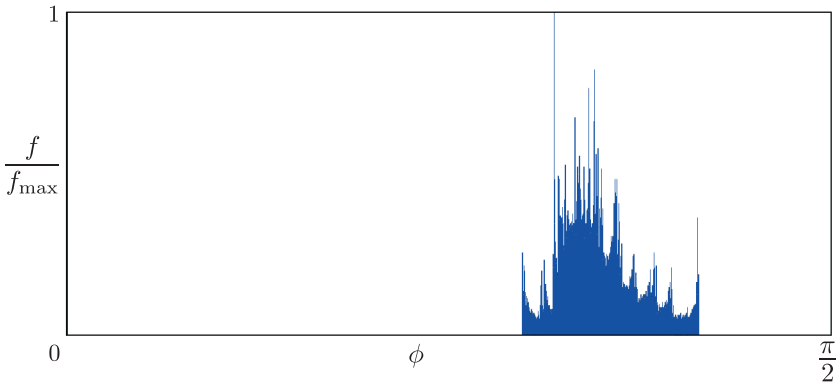

Fig. 5. Histogram for verification of the criterion of angles for the attractor of the Poincaré map of the system (4.1), (4.2) at $\mu = 0.3$, $T = 4$.

4.2. A System of Two Interacting Particles Placed on Alternately Rotating Disks

Another system introduced in [35] is composed of two disks placed horizontally, one above the other, which rotate about the common axis alternately (while one rotates, the other is at rest and vice versa) with angular velocity ω. On each disk a particle is placed, capable of sliding on it with the friction force proportional to its velocity relative to the disk with coefficient α. Suppose that there is a potential field $U(r)$ symmetric about the axis, with potential minimum at the center and strongly growing to the edges of the disks. In addition, assume that the particles interact via a potential field $V(\mathbf{r}_1 - \mathbf{r}_2)$, where $\mathbf{r}_1 = (x_1, y_1)$ and $\mathbf{r}_2 = (x_2, y_2)$ are their position vectors. Concretely, the fields are defined as

$$U(x,y) = \frac{1}{2}k(x^2+y^2) + \frac{1}{4}(x^2+y^2)^2 \tag{4.5}$$

and

$$V(x,y) = \varepsilon\Big(-\frac{1}{3}x^3 + xy^2\Big). \tag{4.6}$$

Then the model set of equations reads

$$\begin{aligned}
\ddot{x}_1 &= x_1(k + x_1^2 + y_1^2) + \alpha(-\omega_1 y_1 - \dot{x}_1) - \varepsilon[(x_1 - x_2)^2 - (y_1 - y_2)^2],\\
\ddot{y}_1 &= y_1(k + x_1^2 + y_1^2) + \alpha(\omega_1 x_1 - \dot{y}_1) + 2\varepsilon(x_1 - x_2)(y_1 - y_2),\\
\ddot{x}_2 &= x_2(k + x_2^2 + y_2^2) + \alpha(-\omega_2 y_2 - \dot{x}_2) + \varepsilon[(x_1 - x_2)^2 - (y_1 - y_2)^2],\\
\ddot{y}_2 &= y_2(k + x_2^2 + y_2^2) + \alpha(\omega_2 x_2 - \dot{y}_2) - 2\varepsilon(x_1 - x_2)(y_1 - y_2),
\end{aligned} \tag{4.7}$$

where

$$\omega_1(t) = \begin{cases} \omega_0, & nT \leqslant t < nT + T/2 \\ 0, & nT + T/2 \leqslant t < nT, \end{cases} \qquad \omega_2(t) = \begin{cases} 0, & nT \leqslant t < nT + T/2 \\ \omega_0, & nT + T/2 \leqslant t < nT. \end{cases}$$

Figure 6 illustrates the dynamics of the model (4.7) at $k = 3$, $\alpha = 3$, $\varepsilon = 0.03$, $T = 16$, $\omega_0 = 2\pi$. Panel (a) shows the time evolution of the spatial position of two particles. Observe that rotations of one and the other particle (red and blue curves) take place alternately, and the motion is not periodic: the forms of the coils are not repeated in successive stages of activity in one and the other subsystem. Panel (b) is a portrait of the attractor in the stroboscopic section as projected

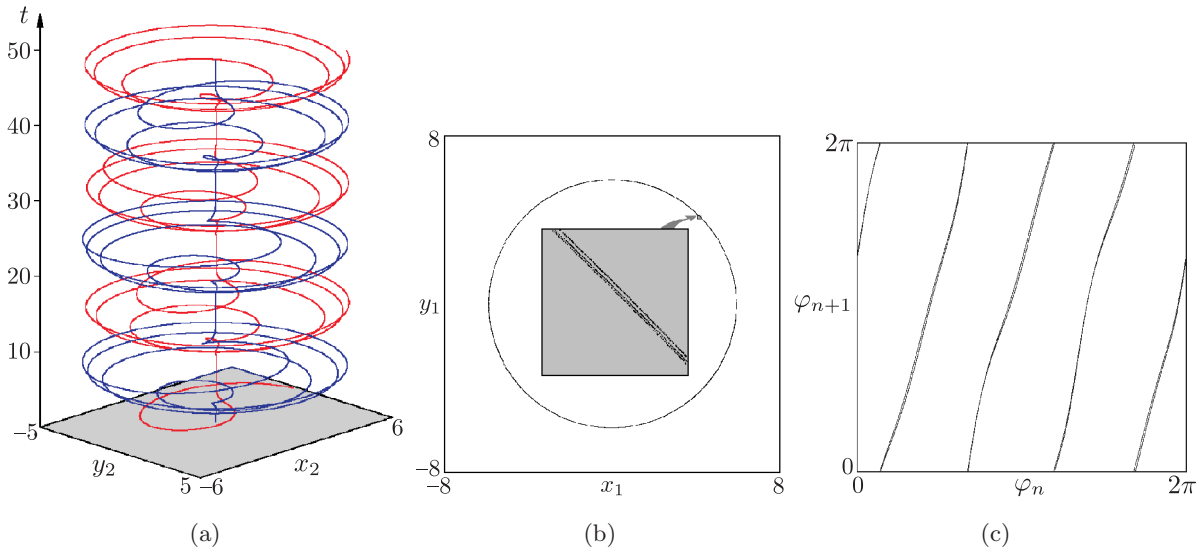

Fig. 6. Time evolution of spatial positions of the particles on the disks (a), attractor projection in the stroboscopic section with magnified fragment illustrating Cantor-like transversal structure (b), and iteration diagram for the angular coordinates of one of the particles (c) computed for the model (4.7) with parameters $k = 3,\ \alpha = 3,\ \varepsilon = 0.03,\ T = 16,\ \omega_0 = 2\pi$.

on the plane of coordinates of one particle $(x_1,\ y_1)$. In the original scale, it looks like a circle, but a zoom reveals distinguishable transversal Cantor-like structure as it is a kind of Smale – Williams solenoid. Indeed, the iteration diagram for the angular coordinate of one of the particles determined immediately after the end of each rotation stage of the corresponding disk behaves in accordance with the expanding circle map. One bypass around the circle for a preimage implies four bypasses for the image. The chaotic nature of the attractor is supported by computation of the spectrum of Lyapunov exponents for the Poincaré map:

$$\begin{aligned} &\Lambda_1 = \quad 1.354,\ \Lambda_2 = -6.90,\quad \Lambda_3 = -7.65,\quad \Lambda_4 = -11.61,\\ &\Lambda_5 = -32.81,\ \Lambda_6 = -32.92,\ \Lambda_7 = -45.34,\ \Lambda_8 = -47.26. \end{aligned} \tag{4.8}$$

Note that the largest exponent is close to ln 4 in accordance with the quadrupling expanding transformation of the angular variable on a period of the rotation switches.

Figure 7 presents results of verification of hyperbolicity of the attractor for the eight-dimensional Poincaré map $\mathbf{x}_{n+1} = \mathbf{f}(\mathbf{x}_n)$ of the model (4.7), via computation of the angles between unstable and stable subspaces for a long reference orbit on the attractor. The numerically obtained histogram demonstrates the absence of angles close to zero confirming that the attractor of the Poincaré map is hyperbolic.

4.3. Parametric Excitation of Standing-wave Patterns by Periodically Modulated Pumping

Parametric excitation of standing-wave patterns on a string [47, 48] may produce chaotic oscillations associated with a hyperbolic attractor as suggested in [49, 50]. The idea is to supply pumping alternately on a low and a high frequency with some modulation period and provide parametric excitation of short-wave and long-wave patterns turn by turn. With appropriately chosen parameters, the transfer of the spatial phase from one pattern to another and back takes place in such a way that over the full period of the pump modulation the phase undergoes a transformation according to the expanding circle map. Due to dissipation, compression of the phase volume in the state space ensures the presence of the attractor of Smale – Williams type.[4)] The easiest way to

[4)] Originally, in the suggested model the triple-expanding map was arranged (see [43] and [44]), but later the possibility of obtaining other odd factors from 5 to 11 [50] was indicated.

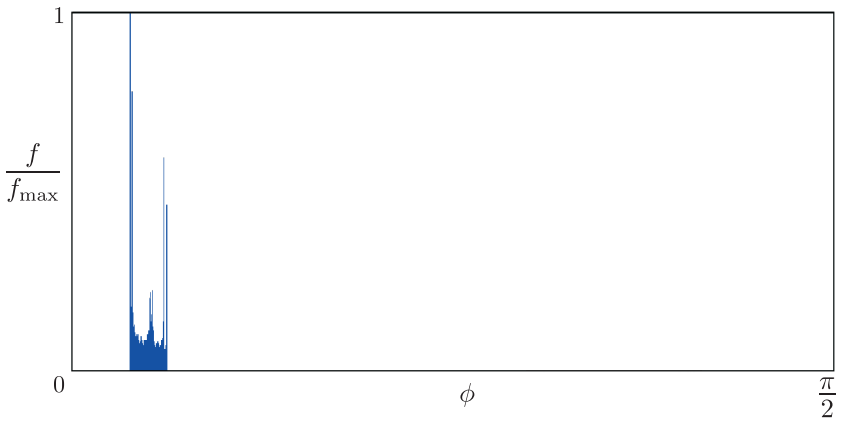

Fig. 7. Verification of the criterion of angles for the attractor of the Poincaré map of system (4.7) with a histogram obtained at $k = 3,\ \alpha = 3,\ \varepsilon = 0.03,\ T = 16,\ \omega_0 = 2\pi$. The stroboscopic Poincaré section in the computations corresponds to time instants $T/4 + nT$, where n is an integer.

implement this idea in a mathematical model is to use a system closed into a ring (although in the experiment it is not the simplest setup to deal with).

Following [49, 50], we postulate the partial differential equation for the model system

$$\begin{aligned}(1+\varepsilon\sin 4k_0x)\frac{\partial^2 y}{\partial t^2} &= -(\alpha+y^2)\frac{\partial y}{\partial t} - \gamma y \\ &+ \left[1 + a_2^0\sin^2\pi(t/T-1/4)\sin 2\omega_0 t + a_6^0\cos^2\pi(t/T-1/4)\sin 6\omega_0 t\right]\frac{\partial^2 y}{\partial x^2},\end{aligned} \tag{4.9}$$

where the normalization used is such that the propagation velocity $c_0 = 1$. The equation is complemented with the boundary condition of periodicity

$$y(x+L,t) \equiv y(x,t). \tag{4.10}$$

Here $\omega_0 = 2\pi c_0/L$ and $k_0 = 2\pi/L$ roughly correspond to the frequency and wave number of the fundamental mode. Parameter ε characterizes spatial inhomogeneity of the mass distribution on the string, a_2^0 and a_6^0 are the amplitudes of low-frequency and high-frequency pumping, which is modulated in time with period T.

Figure 8a illustrates the space-time evolution of patterns obtained from numerical integration of the partial differential equation at parameters assigned as

$$\omega_0 = 2\pi,\ k_0 = 2\pi,\ \ L = 1,\ \ T = 40,\ \ a_2^0 = 0.4,\ a_6^0 = 0.2,\ \varepsilon = 0.2,\ \alpha = 0.4,\ \gamma = 0.03. \tag{4.11}$$

The spatial distributions are shown at each next period of fast oscillations, so the high-frequency component is not visible. In the system alternately long-wave and short-wave patterns arise. Their spatial phases from one to another period of pump modulation evolve in accordance with the triple-expanding circle map due to the mechanism described in [49] and [50]. Because of dissipation, the attractor in the stroboscopic map is a Smale – Williams solenoid; in this case it is embedded in an infinite-dimensional phase space of the distributed system.

Verification of the criterion of angles (like some other data-processing techniques developed for finite-dimensional systems) would require a special reformulation for distributed systems described by partial differential equations. As an alternative, in our case it is possible to turn to a reduced finite-dimensional model [35, 51], which gives a fairly good description of the system dynamics.

In view of the fact that the parametric excitation takes place at the wave numbers k_0 and $3k_0$, it is natural to consider a model where the dynamical variables are represented by time-dependent coefficients of expansion of the string instant profile over these spatial modes. So, we use a substitution

$$y(x,t) = u_1(t)\cos k_0x + v_1(t)\sin k_0x + u_3(t)\cos 3k_0x + v_3(t)\sin 3k_0x, \tag{4.12}$$

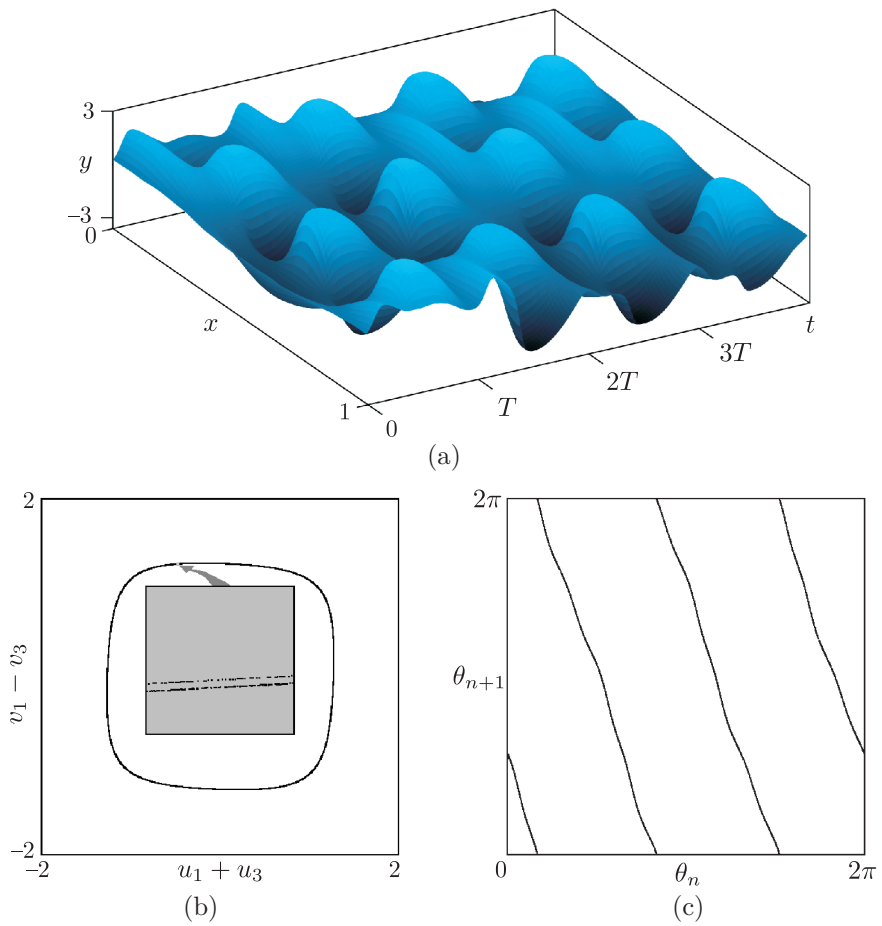

Fig. 8. Space-time diagram illustrating the dynamics of the distributed system (4.9) with boundary conditions of periodicity (4.10) on four modulation periods (a), stroboscopic portrait of the attractor in two-dimensional projection for the reduced model (4.13) (b), and iteration diagram for the angular variable obtained for the reduced model (4.13). Parameters of the system are assigned according to (4.11).

and then multiply both sides of equation (2.1) by $\cos k_0 x$, $\sin k_0 x$, $\cos 3k_0 x$ and $\sin 3k_0 x$, each time performing integration over the spatial period. As a result, we obtain a set of equations for the coefficients:

$$\ddot{u}_1 = \frac{f_1 - \frac{1}{2}\varepsilon g_3}{1 - \frac{1}{4}\varepsilon^2}, \quad \ddot{u}_3 = \frac{f_3 - \frac{1}{2}\varepsilon g_1}{1 - \frac{1}{4}\varepsilon^2}, \quad \ddot{v}_1 = \frac{g_1 - \frac{1}{2}\varepsilon f_3}{1 - \frac{1}{4}\varepsilon^2}, \quad \ddot{v}_3 = \frac{g_3 - \frac{1}{2}\varepsilon f_1}{1 - \frac{1}{4}\varepsilon^2}, \tag{4.13}$$

where

$$\begin{aligned} f_1 = {} & -\omega_0^2 \left(1 + a_2(t)\sin 2\omega_0 t + a_6(t)\sin 6\omega_0 t\right) u_1 - \gamma u_1 - \alpha \dot{u}_1 \\ & - \frac{1}{2}\Big[\Big(\frac{3}{2}u_1^2 + u_1 u_3 + u_3^2 + \frac{1}{2}v_1^2 + v_1 v_3 + v_3^2\Big)\dot{u}_1 + \frac{1}{2}(u_1^2 + 4u_1 u_3 - v_1^2)\dot{u}_3 \\ & + (u_1 v_1 - u_3 v_1 + u_1 v_3)\dot{v}_1 + (u_1 v_1 + 2u_1 v_3)\dot{v}_3\Big], \end{aligned}$$

$$\begin{aligned} g_1 = {} & -\omega_0^2 \left(1 + a_2(t)\sin 2\omega_0 t + a_6(t)\sin 6\omega_0 t\right) v_1 - \gamma v_1 \\ & - \alpha \dot{v}_1 - \frac{1}{2}\Big[\Big(\frac{3}{2}v_1^2 - v_1 v_3 + v_3^2 + \frac{1}{2}u_1^2 - u_1 u_3 + u_3^2\Big)\dot{v}_1 + \frac{1}{2}(u_1^2 + 4v_1 v_3 - v_1^2)\dot{v}_3 \\ & + (u_1 v_1 - u_3 v_1 + u_1 v_3)\dot{u}_1 + (-u_1 v_1 + 2u_3 v_1)\dot{u}_3\Big], \end{aligned}$$

$$f_3 = -9\omega_0^2\,(1 + a_2(t)\sin 2\omega_0 t + a_6(t)\sin 6\omega_0 t)\,u_3 - \gamma u_3 - \alpha\dot{u}_3$$
$$- \frac{1}{4}\left[(u_1^2 + 4u_1u_3 - v_1^2)\dot{u}_1 + 2(-u_1v_1 + 2u_3v_1)\dot{v}_1 + (2u_1^2 + 2v_1^2 + 3u_3^2 + v_3^2)\dot{u}_3 + 2u_3v_3\dot{v}_3\right],$$

$$g_3 = -9\omega_0^2\,(1 + a_2(t)\sin 2\omega_0 t + a_6(t)\sin 6\omega_0 t)\,v_3 - \gamma v_3 - \alpha\dot{v}_3$$
$$- \frac{1}{4}\left[2(u_1v_1 + 2u_1v_3)\dot{u}_1 + (u_1^2 + 4v_1v_3 - v_1^2)\dot{v}_1 + 2u_3v_3\dot{u}_3 + (2u_1^2 + 2v_1^2 + u_3^2 + 3v_3^2)\dot{v}_3\right].$$

Results of numerical simulations for the reduced system (4.13) appear to be in good agreement with the computations based on the partial differential equation (4.9). In particular, at parameters (4.11) the amplitudes of the sine and cosine components (which are associated with the spatial phase of the standing waves in the original system) evolve in time chaotically. Panel (b) of Fig. 8 shows the attractor of the reduced model in stroboscopic section as projected on the plane of variables $(u_1 + u_3,\, v_1 - v_3)$, which correspond to variables $(y(0,1),\, y(L/4,t))$ of the original system. Observe the transversal Cantor-like structure visible under magnification. Panel (c) shows the iteration diagram for the spatial phases defined for the reduced model as $\theta_n = \arg\,[u_1(nT) + iv_1(nT)]$ at $t = nT$. It corresponds to the triple expanding circle map responsible for the occurrence of the Smale-Williams attractor.

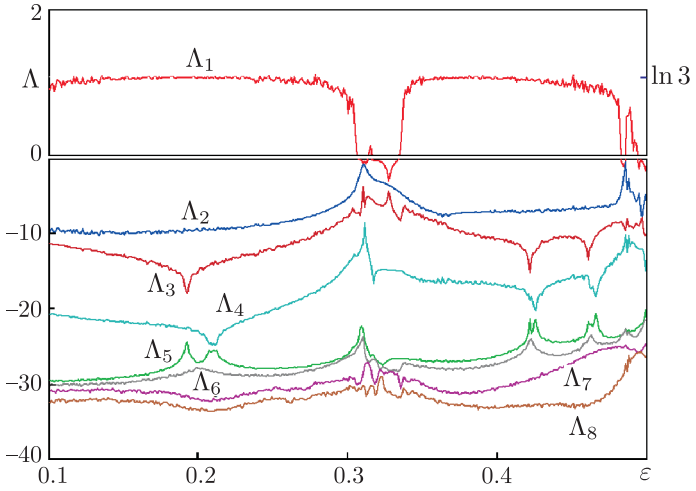

Fig. 9. Lyapunov exponents for the reduced model of the parametrically excited string (4.13) depending on the parameter of mass inhomogeneity distribution. Other parameters: $\omega_0 = 2\pi$, $k_0 = 2\pi$, $T = 40$, $L = 1$, $a_2^0 = 0.4$, $a_6^0 = 0.2$, $\alpha = 0.4$, $\gamma = 0.03$.

Figure 9 shows a plot of Lyapunov exponents for the reduced model depending on the parameter of inhomogeneity of the mass distribution. Intervals in which the largest Lyapunov exponent is approximately constant and close to the value $\Lambda_1 \approx \ln 3$ correspond to the hyperbolic chaos, when the Poincaré map possesses an attractor of the Smale – Williams type, with the triple expanding circle map for the angular coordinate. In ranges where significant deviations from this value occur, hyperbolicity is apparently violated; characteristic for these domains is the presence of drops in the Lyapunov exponent plot corresponding to windows of periodicity.

Now we may verify the criterion of angles for the reduced model (4.13) referring to the eight-dimensional stroboscopic Poincaré map according to the scheme described in Section 2. Figure 10 shows histograms for distributions of the angles between stable and unstable subspaces for trajectories on the attractors in the case of hyperbolic dynamics (a), and in the case when the attractor is nonhyperbolic (b) and angles close to zero are observed with notable probability.

For parameters assigned in accordance with (4.11) the distribution of angles is separated from zero, i. e., the test confirms the hyperbolic nature of the attractor of the Poincaré map of the reduced model. Having in mind good agreement of the dynamics of the original system (4.9) and of the finite-dimensional reduced model (4.13) and taking into account the roughness of the hyperbolic

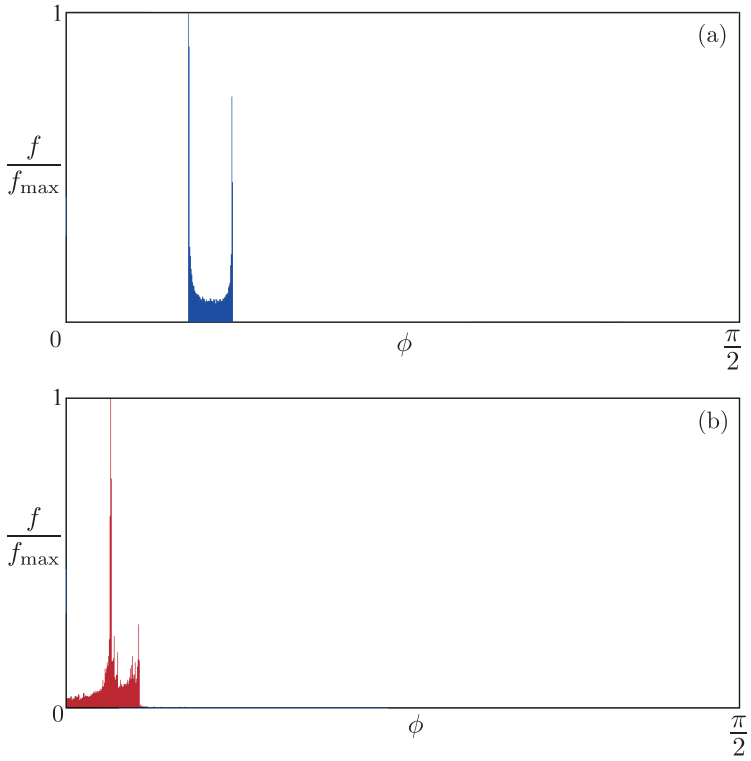

Fig. 10. Histograms for verification of the criterion of angles for the reduced model (4.13) obtained at $\omega_0 = 2\pi,\ k_0 = 2\pi,\ T = 40,\ L = 1,\ \alpha$=0.4, $a_2^0 = 0.4,\ a_6^0 = 0.2,\ \gamma = 0.03,\ \varepsilon = 0.2$ (a) and $\varepsilon = 0.49$ (b). In the first case the attractor is hyperbolic, in the second case the test indicates the presence of zero angles, which imply tangencies of stable and unstable manifolds, and the attractor is nonhyperbolic.

attractor of the Poincaré map, this result may be regarded as an argument in favor of the hyperbolic nature of the attractor of the original distributed system as well.

5. CONCLUSION

To verify the hyperbolic nature of attractors for model mechanical systems, we implement and test a method based on statistics of angles between the stable and unstable manifolds. For this purpose, on some reference trajectory belonging to the attractor the angles between the stable and unstable subspaces of infinitesimal perturbation vectors are evaluated, and their statistical distribution is analyzed. We demonstrate that for several mechanical systems with an appropriate selection of the parameters the analysis demonstrates the absence of angles close to zero, indicating that the corresponding attractors are hyperbolic. In the models under study these are different versions of the Smale – Williams solenoids in the Poincaré maps as seen from the topology of iterative diagrams for the angular variables, corresponding to the expanding circle maps. To be accurate, we admit that at present the arguments in favor of the hyperbolic nature of the attractors are based on qualitative analysis and numerical results. A more rigorous mathematical justification of the hyperbolicity, for example, with the verification criterion of cones [52–54], is desirable, and may be one of the directions for further studies.

ACKNOWLEDGMENTS

This work was supported by RSF grant No 15-12-20035.

REFERENCES

1. Smale, S., Differentiable Dynamical Systems, *Bull. Amer. Math. Soc.,* 1967, vol. 73, pp. 747–817.
2. Williams, R. F., Expanding Attractors, *Publ. Math. Inst. Hautes Études Sci.,* 1974, vol. 43, pp. 169–203.
3. *Dynamical Systems 9: Dynamical Systems with Hyperbolic Behaviour,* D. V. Anosov (Ed.), Encyclopaedia Math. Sci., vol. 66, Berlin: Springer, 1995.
4. Katok, A. and Hasselblatt, B., *Introduction to the Modern Theory of Dynamical Systems,* Encyclopedia Math. Appl., vol. 54, Cambridge: Cambridge Univ. Press, 1995.
5. Afraimovich, V. and Hsu, S.-B., *Lectures on Chaotic Dynamical Systems,* AMS/IP Stud. Adv. Math., vol. 28, Providence, R.I.: AMS, 2003.
6. Bonatti, Ch., Díaz, L. J., and Viana, M., *Dynamics beyond Uniform Hyperbolicity: A Global Geometric and Probobalistic Perspective,* Encyclopaedia Math. Sci., vol. 102, Berlin: Springer, 2005.
7. Andronov, A. and Pontryagin, L., Systèmes grossiers, *Dokl. Akad. Nauk. SSSR,* 1937, vol. 14, no. 5, pp. 247–250 (Russian).
8. Andronov, A. A., Vitt, A. A., and Khaĭkin, S. E., *Theory of Oscillators,* New York: Pergamon, 1966.
9. Rabinovich M. I. and Gaponov-Grekhov, A. V., Problems of Present-Day Nonlinear Dynamics, *Her. Russ. Acad. Sci.,* 1997, vol. 67, no. 4, pp. 257–262; see also: *Vestn. Ross. Akad. Nauk,* 1997, vol. 67, no. 7, pp. 608–614.
10. Shilnikov, L. P., Shilnikov, A. L., Turaev, D., and Chua, L. O., *Methods of Qualitative Theory in Nonlinear Dynamics: Part 1,* World Sci. Ser. Nonlinear Sci. Ser. A Monogr. Treatises, vol. 4, River Edge, N.J.: World Sci., 1998.
11. Shilnikov, L. P., Shilnikov, A. L., Turaev, D., and Chua, L. O., *Methods of Qualitative Theory in Nonlinear Dynamics: Part 2,* World Sci. Ser. Nonlinear Sci. Ser. A Monogr. Treatises, vol. 5, River Edge, N.J.: World Sci., 2001.
12. Afraimovich, V. S., Gonchenko, S. V., Lerman, L. M., Shilnikov, A. L., and Turaev, D. V., Scientific Heritage of L. P. Shilnikov, *Regul. Chaotic Dyn.,* 2014, vol. 19, no. 4, pp. 435–460.
13. Kuznetsov, A. P., Kuznetsov, S. P., and Ryskin, N. M., *Nonlinear Oscillations,* Moscow: Fizmatlit, 2002 (Russian).
14. Borisov, A. V., Kazakov, A. O., and Kuznetsov, S. P., Nonlinear Dynamics of the Rattleback: A Nonholonomic Model, *Physics–Uspekhi,* 2014, vol. 57, no. 5, pp. 453–460; see also: *Uspekhi Fiz. Nauk,* 2014, vol. 184, no. 5, pp. 493–500.
15. Gonchenko, A. S., Gonchenko, S. V., and Kazakov, A. O., Richness of Chaotic Dynamics in Nonholonomic Models of a Celtic Stone, *Regul. Chaotic Dyn.,* 2013, vol. 18, no. 5, pp. 521–538.
16. Kuznetsov, S. P., Plate Falling in a Fluid: Regular and Chaotic Dynamics of Finite-Dimensional Models, *Regul. Chaotic Dyn.,* 2015, vol. 20, no. 3, pp. 345–382.
17. Monin, A. S., On the Nature of Turbulence, *Sov. Phys. Usp.,* 1978, vol. 21, no. 5, pp. 429–442; see also: *Uspekhi Fiz. Nauk,* 1978, vol. 125, no. 5, pp. 97–122.
18. Letellier, Ch., *Chaos in Nature,* Singapore: World Sci., 2013.
19. Scott, S. K., *Chemical Chaos,* Oxford: Oxford Univ. Press, 1993.
20. Thompson, J. M. T. and Stewart, H. B., *Nonlinear Dynamics and Chaos,* New York: Wiley, 1986.
21. Landa, P. S., *Nonlinear Oscillations and Waves in Dynamical Systems,* Dordrecht: Springer, 1996.
22. Shannon, C. E., A Mathematical Theory of Communication, *Bell Syst. Tech. J.,* 1948, vol. 27, pp. 379–423, 623–656.
23. Kuznetsov, S. P., Example of a Physical System with a Hyperbolic Attractor of the Smale – Williams Type, *Phys. Rev. Lett.,* 2005, vol. 95, no. 14, 144101, 4 pp.
24. Kuznetsov, S. P. and Seleznev, E. P., Strange Attractor of Smale – Williams Type in the Chaotic Dynamics of a Physical System, *J. Exp. Theor. Phys.,* 2006, vol. 102, no. 2, pp. 355–364; see also: *Zh. Èksper. Teoret. Fiz.,* 2006, vol. 129, no. 2, pp. 400–412.
25. Isaeva, O. B., Jalnine, A. Yu., and Kuznetsov, S. P., Arnold's Cat Map Dynamics in a System of Coupled Nonautonomous van der Pol Oscillators, *Phys. Rev. E,* 2006, vol. 74, no. 4, 046207, 5 pp.
26. Kuznetsov, S. P. and Pikovsky, A., Autonomous Coupled Oscillators with Hyperbolic Strange Attractors, *Phys. D,* 2007, vol. 232, no. 2, pp. 87–102.
27. Kuznetsov, S. P., Example of Blue Sky Catastrophe Accompanied by a Birth of Smale – Williams Attractor, *Regul. Chaotic Dyn.,* 2010, vol. 15, nos. 2–3, pp. 348–353.
28. Kuznetsov, S. P., *Hyperbolic Chaos: A Physicist's View,* Berlin: Springer, 2012.
29. Kuznetsov, S. P., Dynamical Chaos and Uniformly Hyperbolic Attractors: From Mathematics to Physics, *Phys. Uspekhi,* 2011, vol. 54, no. 2, pp. 119–144; see also: *Uspekhi Fiz. Nauk,* 2011, vol. 181, no. 2, pp. 121–149.
30. Kuznetsov, S. P., Plykin Type Attractor in Electronic Device Simulated in MULTISIM, *Chaos,* 2011, vol. 21, no. 4, 043105, 10 pp.
31. Isaeva, O. B., Kuznetsov, S. P., and Mosekilde, E., Hyperbolic Chaotic Attractor in Amplitude Dynamics of Coupled Self-Oscillators with Periodic Parameter Modulation, *Phys. Rev. E.,* 2011, vol. 84, no. 1, 016228, 10 pp.

32. Isaeva, O. B., Kuznetsov, S. P., Sataev, I. R., Savin, D. V., and Seleznev, E. P., Hyperbolic Chaos and Other Phenomena of Complex Dynamics Depending on Parameters in a Nonautonomous System of Two Alternately Activated Oscillators, *Internat. J. Bifur. Chaos Appl. Sci. Engrg.,* 2015, vol. 25, no. 12, 1530033, 15 pp.
33. Kuznetsov, S. P., Ponomarenko, V. I., and Seleznev, E. P., Autonomous System Generating Hyperbolic Chaos: Circuit Simulation and Experiment, *Izv. Vyssh. Uchebn. Zaved. Prikl. Nelin. Dinam.,* 2013, vol. 21, no. 5, pp. 17–30 (Russian).
34. Jalnine, A. Yu., Hyperbolic and Non-Hyperbolic Chaos in a pair of Coupled Alternately Excited FitzHugh – Nagumo Systems, *Commun. Nonlinear Sci. Numer. Simul.,* 2015, vol. 23, nos. 1–3, pp. 202–208.
35. Kuznetsov, S. P., Some Mechanical Systems Manifesting Robust Chaos, *Nonlinear Dynamics & Mobile Robotics,* 2013, vol. 1, no. 1, pp. 3–22.
36. Kuznetsov, S. P., Hyperbolic Strange Attractors of Physically Realizable Systems, *Izv. Vyssh. Uchebn. Zaved. Prikl. Nelin. Dinam.,* 2009, vol. 17, no. 4, pp. 5–34 (Russian).
37. Hénon, M., A Two-Dimensional Mapping with a Strange Attractor, *Commun. Math. Phys.,* 1976, vol. 50, no. 1, pp. 69–77.
38. Lai, Y.-Ch., Grebogi, C., Yorke, J. A., and Kan, I., How Often Are Chaotic Saddles Nonhyperbolic?, *Nonlinearity,* 1993, vol. 6, no. 5, pp. 779–798.
39. Anishchenko, V. S., Kopeikin, A. S., Kurths, J., Vadivasova, T. E., Strelkova, G. I., Studying Hyperbolicity in Chaotic Systems, *Phys. Lett. A,* 2000, vol. 270, no. 6, pp. 301–307.
40. Ginelli, F., Poggi, P., Turchi, A., Chaté, H., Livi, R., and Politi, A., Characterizing Dynamics with Covariant Lyapunov Vectors, *Phys. Rev. Lett.,* 2007, vol. 99, no. 13, 130601, 4 pp.
41. Kuptsov, P. V., Fast Numerical Test of Hyperbolic Chaos, *Phys. Rev. E,* 2012, vol. 85, no. 1, 015203, 4 pp.
42. Kuznetsov, S. P., Hyperbolic Chaos in Self-Oscillating Systems Based on Mechanical Triple Linkage: Testing Absence of Tangencies of Stable and Unstable Manifolds for Phase Trajectories, *Regul. Chaotic Dyn.,* 2015, vol. 20, no. 6, pp. 649–666.
43. Kuznetsov, S. P. and Turukina, L. V., Attractors of Smale – Williams Type in Periodically Kicked Model Systems, *Izv. Vyssh. Uchebn. Zaved. Prikl. Nelin. Dinam.,* 2010, vol. 18, no. 5, pp. 80–92 (Russian).
44. Benettin, G., Galgani, L., Giorgilli, A., and Strelcyn, J.-M., Lyapunov Characteristic Exponents for Smooth Dynamical Systems and for Hamiltonian Systems: A Method for Computing All of Them: P. 1: Theory; P. 2: Numerical Application, *Meccanica,* 1980, vol. 15, pp. 9–30.
45. Schuster, H. G. and Just, W., *Deterministic Chaos: An Introduction,* Weinheim: Wiley-VCH, 2005.
46. Kuznetsov, S. P., *Dynamical Chaos,* 2nd ed., Moscow: Fizmatlit, 2006 (Russian).
47. Rayleigh, J. W. S., *The Theory of Sound, Volume One,* 2nd ed., New York: Dover, 2013.
48. Rowland, D. R., Parametric Resonance and Nonlinear String Vibrations, *Am. J. Phys.,* 2004, vol. 72, no. 6, pp. 758–766.
49. Isaeva, O. B., Kuznetsov, A. S., and Kuznetsov, S. P., Hyperbolic Chaos of Standing Wave Patterns Generated Parametrically by a Modulated Pump Source, *Phys. Rev. E,* 2013, vol. 87, no. 4, 040901(R), 4 pp.
50. Isaeva, O. B., Kuznetsov, A. S., and Kuznetsov, S. P., Hyperbolic Chaos in Parametric Oscillations of a String, *Nelin. Dinam.,* 2013, vol. 9, no. 1, pp. 3–10 (Russian).
51. Kuznetsov, S. P., Kuznetsov, A. S., and Kruglov, V. P., Hyperbolic Chaos in Systems with Parametrically Excited Patterns of Standing Waves, *Nelin. Dinam.,* 2014, vol. 10, no. 3, pp. 265–277 (Russian).
52. Sinaĭ, Ya. G., The Stochasticity of Dynamical Systems: Selected Translations, *Selecta Math. Soviet.,* 1981, vol. 1, no. 1, pp. 100–119.
53. Kuznetsov, S. P. and Sataev, I. R., Hyperbolic Attractor in a System of Coupled Non-Autonomous van der Pol Oscillators: Numerical Test for Expanding and Contracting Cones, *Phys. Lett. A,* 2007, vol. 365, nos. 1–2, pp. 97–104.
54. Wilczak, D., Uniformly Hyperbolic Attractor of the Smale – Williams Type for a Poincaré Map in the Kuznetsov System: With Online Multimedia Enhancements, *SIAM J. Appl. Dyn. Syst.,* 2010, vol. 9, no. 4, pp. 1263–1283.